Journal of Catalysis 271 (2010) 370–385

Contents lists available at ScienceDirect

Journal of Catalysis

journal homepage: www.elsevier.com/locate/jcat

Identity and chemical function of gallium species inferred from microkinetic modeling studies of propane aromatization over Ga/HZSM-5 catalysts

Gowri Krishnamurthy [a], Aditya Bhan [b], W. Nicholas Delgass [a,*]

[a] School of Chemical Engineering, 480 Stadium Mall Drive, West Lafayette, IN 47907-1283, USA
[b] Department of Chemical Engineering and Materials Science, 421 Washington Avenue SE, Minneapolis, MN 55455, USA

ARTICLE INFO

Article history:
Received 4 December 2009
Revised 3 February 2010
Accepted 22 February 2010
Available online 8 April 2010

Keywords:
Alkane aromatization
Propane
Gallium
ZSM-5
Kinetic modeling

ABSTRACT

Ga/HZSM-5 catalysts, synthesized by the incipient wetness impregnation technique, showed a steady decline in Brønsted acidity with gallium addition. A maximum in propane conversion and aromatics selectivity at a Ga/Al ratio of about 0.5 suggests synergy between proton and gallium sites. A microkinetic model using 312 elementary steps and 25 rate and equilibrium parameters to describe the aromatization of propane over HZSM-5 with Si/Al of 16 is the base case against which the effects of Ga are compared. Kinetic models based on two different Ga active sites, including GaH^{2+} and GaH_2^+, were first used individually to describe the diverse dataset that includes conversion to 10 different products as a function of temperature (510–540 °C), space time (2–8 g_{cat} h/mol), and Ga/Al (0–1) variations. An evaluation of these models based on an assigned catalytic functionality for these sites and the associated parameters showed that both sites are required to provide a unified description of the catalytic behavior across gallium content with monohydridic Ga-sites being predominantly prevalent at low Ga/Al ratio and dihydridic Ga-sites at high Ga/Al ratios. In this paper, we address the ability to discriminate between the models and their implications for the primarily dehydrogenation nature of the Ga active sites.

1. Introduction

Increasing global competition and demand for energy resources put a premium on increased efficiency in catalyst design. We approach the catalyst design problem with a methodology called Discovery Informatics [1], an iterative model-building approach to extract knowledge from data (Fig. 1). A crucial piece of this framework is a forward model that captures the kinetic information in the data via a microkinetic model and then links the kinetic model to a catalyst chemistry model that connects quantitative chemical and structural descriptors, including Si/Al ratio, metal content, and catalyst structure to the rate constants via Polanyi relations, expert rules, and any other available information. Once the forward model has been developed, an inverse search can be undertaken to predict the descriptor set that would lead to the desired catalyst performance.

A medium for demonstrating this methodology is the aromatization of propane over ZSM-5-based catalysts. The activation of relatively stable light alkanes and their selective conversion to value-added products, aromatics, and hydrogen, has received significant attention over the last few decades [2–5], given the scientific challenges involved and the commercial incentives for gasoline additives and raw materials for the petrochemicals industry. ZSM-5 with its high surface area, well-defined porosity at a favorable size, high thermal stability, intrinsic acidity, and high resistance to deactivation serves as the catalyst system of choice. A drawback of the highly acidic HZSM-5 is the high concentration of hydrogen-rich C_1–C_2 alkanes in the outlet stream as a result of protolytic cracking. It has been shown that the presence of extra-framework metals in HZSM-5 can enhance the dehydrogenation ability of the catalyst [7,11–16], thereby increasing the amount of olefins formed that can then oligomerize and cyclize to produce aromatics. The higher dehydrogenation rate also implies a lower cracking rate due to the release of molecular hydrogen instead of hydrogen-rich fuel gases from hydrides. Different extra-framework metals including Zn [6], Pt [7–10] and Ga [7,11–16] have been reported to enhance propane dehydrogenation rates in the literature. The deactivation of Pt/HZSM-5 and instability of Zn/HZSM-5 formulations encouraged the use of Ga/HZ5M-5 as our system of interest.

Microkinetic analysis, popularized by Dumesic et al. [17], involves the use of a set of elementary reaction steps and fundamental concepts to describe the reaction events involved. Adjusting the parameters of that description to fit experimental data thus produces a quantitative understanding of complex surface reaction networks. The coupling of the hydrocarbon chemistry and the large dimensionality of the aromatization reaction system poses significant challenges.

* Corresponding author. Fax: +1 765 494 0805.
E-mail address: delgass@ecn.purdue.edu (W.N. Delgass).

0021-9517/$ - see front matter © 2010 Elsevier Inc. All rights reserved.
doi:10.1016/j.jcat.2010.02.026

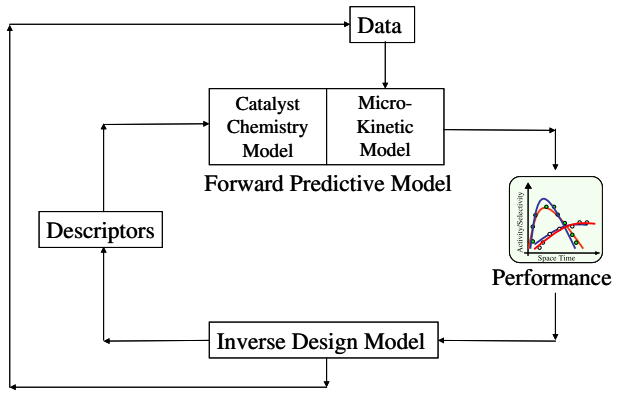

Fig. 1. The discovery informatics methodology.

The goal of this paper is to develop a mechanistic understanding of propane aromatization over Ga/HZSM-5 catalysts. The introduction of gallium in HZSM-5 increases the dehydrogenation rate and has been found to be a significant improvement over HZSM-5 catalysts in increasing the selectivity to aromatics. An optimum gallium loading has been reported by many researchers, indicating a synergistic interplay between the gallium and proton active sites [10,14,15,18–20]. The chemical nature and role of the active gallium site have been addressed by several researchers. Initially, it was believed that Ga_2O_3 was the active catalytic species. However, kinetic results coupled with X-ray diffraction and thermo-gravimetric analyses have proved that the activity of Ga_2O_3–HZSM-5 is much higher than that of Ga_2O_3 alone [19,21]. The predominant viewpoint in the literature is that gallium annihilates proton sites, and the two act in concert during propane aromatization [10,14,15,22,23]. Different propositions on the chemical nature of gallium, including Ga^+ [11,16], GaO^+ [7,14,24,25,52], and GaH_2^+ [24,25] have been made. The presence of the GaH_x species was confirmed based on *in situ* Ga K-edge X-ray absorption spectroscopy [23], XANES [26,27], and DRIFTS [28].

Density functional theory (DFT) predictions by Joshi and Thomson [25] suggest the coexistence of the gallium monohydride (GaH^{2+}) species, where one gallium atom replaces two nearby Brønsted acid sites, and GaH_2^+ and Ga^+ species in which one gallium atom replaces a single Brønsted acid site depending on Al proximity and hydrogen partial pressure and temperature. The ethane dehydrogenation activation energy associated with the gallium monohydride site with an Al–Al distance of 0.453 nm was found to be 168 kJ/mol (40 kcal/mol), in good agreement with the experimentally reported value [50] of 39 kcal/mol. This work also suggests the likelihood of an optimum Si/Al ratio. Pidko et al. [29] used DFT calculations to evaluate the relative stabilities of the sites proposed by Joshi and Thomson [25] and suggest that at Al–Al distances >0.814 nm, gallium exists mainly as Ga^+ and partly as the less stable GaH_2^+ and confirm the presence of a H—Ga—$C_2H_5^+$-like species as the reaction intermediate. At an Al–Al distance of 0.484 nm, Pidko et al. propose the predominant presence of highly active GaH^{2+} species, which decomposes to the Ga^+ species with lower activity during the catalytic cycle. In that work, ethane dehydrogenation was found to take place on Ga^+ with an activation energy of 233 kJ/mol, 40 kJ/mol higher than the activation energy on the GaH_2^+ site.

In a recent series of studies, Hensen, van Santen, and coworkers [31] have investigated the aromatization activity of reduced and oxidized Ga/HZSM-5 catalysts. Kazansky et al. [26,27] showed, using DRIFT spectroscopy, that all the protons in HZSM-5 can be replaced by Ga^+ and that these ions can be reversibly oxidized using nitrous oxide. They also used CO-probe DRIFT spectroscopy to identify the various Ga species in the micropores. Kuzmin et al. [30] performed DFT calculations to validate the higher hydrogen–deuterium exchange rate over Ga/HZSM-5 oxidized in N_2O than over Ga/HZSM-5 reduced in H_2. They ascribed the difference to the easy dissociation of H_2 over GaO^+ to give the catalytically active $[GaH(OH)]^+$ cations as opposed to the difficult regeneration of the active GaH_2^+ species from Ga^+. The reaction over neutral gallium oxide particles, $HGa(OH)_2$, was shown to have least activity. Recently, Pidko et al. [31], in their DFT study, considered the gallyl ion, GaO^+, as the active site for ethane dehydrogenation on oxidized Ga/HZSM-5. They proposed the activation of ethane by two parallel pathways. The first was the "alkyl" pathway and involves the formation of the C_2H_5–Ga–OH^+ species from which ethylene can desorb to form H–Ga–OH^+. The second pathway was the "carbenium" pathway, involving the formation of the H—Ga—$OC_2H_5^+$ species with a hydride atom and an alkoxyl group bound to gallium. The adsorbed ethoxy could desorb ethylene. However, they showed that the regeneration of the active GaO^+ by H_2 desorption from H–Ga–OH^+ was not favorable.

Hensen and coworkers [32] have been able to regenerate the GaO^+ species by the addition of steam to Ga/HZSM-5 and reported stable catalytic activity for at least 4 h while co-feeding water. Based on X-ray absorption fine structure (EXAFS) spectroscopy at the Ga K edge, they attributed the increased activity to the formation of a binuclear hydroxyl-bridged Ga reaction intermediate, $[(H)Ga(OH)_2Ga(H)]^{2+}$, that is stabilized by the eight-membered ring of ZSM-5. The bridging hydroxyl bond in the intermediate was also found to be highly acidic, thus leading to an increased hydrogen recombination rate for the binuclear species. Some of the Brønsted acid sites were regenerated by the complete hydrolysis of the gallium species as was demonstrated by the observed increase in concentrations of methane and ethylene, products of cracking reactions. Recently, binuclear gallium oxide clusters, $[Ga_2O_2]_2^+$, stabilized on two spatially separated aluminum ions in oxidized gallium-substituted HZSM-5 and MOR, have been further studied by Pidko et al. using DFT calculations [52,53].

In a recent study, Rane et al. [49] have probed the cracking of *n*-heptane over Ga/HZSM-5 prepared by incipient wetness impregnation, ion exchange, and CVD with $Ga(CH_3)_3$ using *in situ* infrared spectroscopy and Ga K-edge X-ray absorption spectroscopy (XAS) and report the highest activity over oxidized Ga/HZSM-5 catalysts prepared by ion exchange with Ga/Al of 0.6. They suggest the coexistence of Ga^+ and GaH^{2+} sites in reduced gallium-modified materials with Ga^+ dominating at high gallium loadings. They also propose a synergy between Brønsted acid sites and gallium dehydrogenation sites. In 2009, Subbotina and Kazansky [54] used IR diffuse reflectance spectroscopy to understand the mechanism of alkane aromatization on Ga/ZSM-5 prepared by chemical vapor deposition with trimethyl gallium. They confirm the complete replacement of Brønsted acid sites by Ga^+, the primary active site, and propose the oxidative addition of alkane on Ga^+ to form $[Ga^{3+}(H)(R)]^+$-type species.

In a series of isotope studies, Iglesia and coworkers [23,33] have proposed that the recombinative desorption of H-adatoms from the surface of ZSM-5 is the kinetically relevant step in dehydrocyclodimerization reactions and that gallium promotes the activity by acting as a "porthole" for hydrogen removal from the catalyst surface. Meitzner et al. [23] used *in situ* Ga K-edge X-ray absorption spectroscopy (XAS) and methyl/double-bond shift isomerization probe reactions to investigate the chemical nature of Ga in gallium-modified HZSM-5. They propose the GaH_x species as the active site indicating the reduction of gallium under reaction conditions from Ga^{3+} to Ga^+. Biscardi et al. [33] report a reduction in the Brønsted acidity of reduced Ga/HZSM-5 at room temperature. However, the authors do not observe a similar decrease in acidity during reaction conditions and hence invoke the neutral

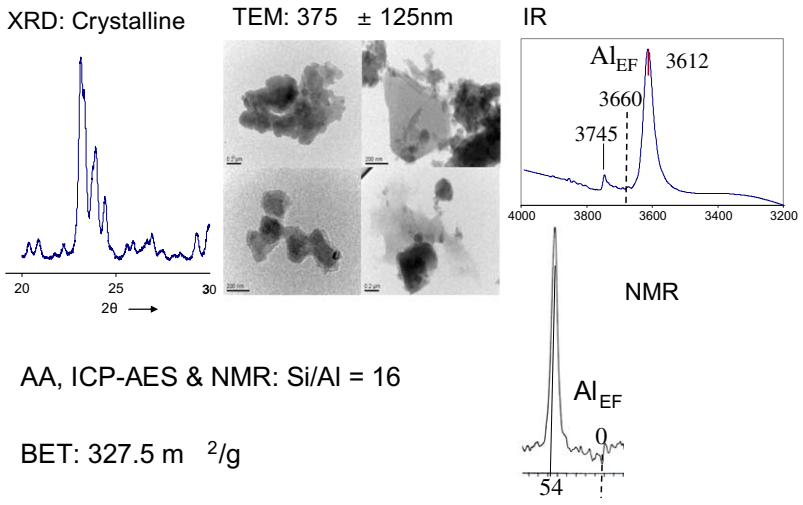

Fig. 2. Properties of the parent HZSM-5: Si/Al = 16.

GaOH species that does not annihilate proton sites, as the active gallium site. All catalytic reactions including C–H activation have been proposed to take place entirely on the acid site. This picture is inconsistent with our kinetic data which indicates an increase in propylene concentration with gallium as well as low aromatics and fuel gas concentrations at high gallium loadings. The kinetic results on our materials point to an increased dehydrogenation function accompanied by a decreased acid function with increasing gallium content. The models we describe in this paper were built to fit the experimental data obtained on our gallium-modified catalysts.

Although several researchers have investigated Ga/HZSM-5 as an aromatization catalyst, the definite nature and functionality of the gallium active site remain to be understood. The possibility of multiple gallium species co-existing under reaction conditions requires a detailed study of each species in order to obtain an overall understanding of the chemistry. Additionally, the gallium functionality cannot be probed in the absence of the proton sites, thereby further convoluting the problem. The objective of this paper is to clarify the chemical nature and kinetic role of gallium in Ga-modified HZSM-5 samples prepared by incipient wetness impregnation. In the next two sections, we describe the experimental and kinetic modeling tools used in the study. We then highlight the results of the experimental and kinetic modeling efforts.

2. Methods

2.1. Experimental

2.1.1. HZSM-5 characterization

HZSM-5 samples used in this study were obtained from ExxonMobil. The structure and crystalline nature were confirmed by X-ray diffraction (XRD), and particle size was measured by transmission electron microscopy (TEM) as 375 ± 125 nm. Both ^{27}Al MAS NMR spectroscopy and room temperature FT-IR spectroscopy confirmed the absence of extra-framework aluminum species as shown in Fig. 2. The Si/Al ratio as measured by atomic absorption spectroscopy and ICP-AES was 16. This value was confirmed by ^{29}Si MAS NMR spectra which led to a Si/Al ratio of 19 on fitting. To observe well-developed NMR signals, catalysts were hydrated over a saturated NH_4Cl solution in a desiccator at 80% relative humidity for a week before MAS NMR spectroscopy. The reference for the ^{27}Al NMR spectra was chosen as the signal of the hydrated Al^{3+} cation in an octahedral environment $[Al(H_2O)_6]^{3+}$. The BET hypothesis, although not an accurate depiction of the microporous system, was used to provide surface area and micro-pore volume estimates of 323.5 ± 5.9 m^2/g and 0.134 cm^3/g, respectively, from N_2 adsorption measurements at 77 K, thus confirming the high porosity of the material.

2.1.2. Preparation of Ga/HZSM-5

Different methods have been used for the introduction of Ga in HZSM-5, including ion exchange and impregnation with gallium salts such as gallium nitrate [18], mechanical mixing with Ga_2O_3 [16,19,34], and chemical vapor deposition with $GaCl_3$ [6] and trimethyl gallium [35]. It was found by X-ray photoelectron spectroscopy (XPS) and electron microscopy that gallium resided primarily on the external surface of catalysts prepared by wet impregnation and incipient wetness impregnation. This was attributed to steric and electrostatic hindrances created due to the hydrated Ga^{3+} cation. It was necessary to disperse the gallium under a reducing environment at high temperatures prior to reactions [18,21,23,36,37]. Even with other preparation techniques, it was found that reduction of Ga/HZSM-5 in H_2 at high temperatures was required to disperse the gallium species into the pores [10,11,14,49].

We found comparable results with the incipient wetness impregnation and ion-exchange techniques and used the incipient wetness impregnation technique with aqueous gallium nitrate solution (Alfa Aesar; 9–10% w/w) to prepare materials with Ga/Al ratio between 0.1 and 1 (corresponding to 0.65 wt.% and 6.5 wt.% Ga). Gallium-modified materials were reduced in H_2 at 530 °C prior to reactions to allow the reduction and migration of Ga species into the pores. A Nicolet Protégé 460 FT-IR spectrometer was used to analyze the OH stretching frequencies at 3610 cm^{-1}, corresponding to Brønsted acid sites, 3660 cm^{-1} representative of extra-framework Al and Ga and 3750 cm^{-1} representative of silanol groups on the external surface or at internal defect sites. The catalyst pellets were heated to 250 °C and cooled down to room temperature in vacuum prior to the IR measurements. Spectra were fit using Origin Pro7 and quantified relative to the 1100 cm^{-1} and 1800 cm^{-1} bands, representative of framework Si–O–Si, as the reference.

2.1.3. Kinetic measurements

Propane aromatization was performed on gallium-modified materials at 1 atm pressure, temperatures ranging from 510 °C to 540 °C, and space times varying from 2 to 8 g_{cat} h/mol with a 100% propane feed. The catalyst temperature was measured with

a thermocouple located in the center of the catalyst bed, and gas flow rates were controlled by Brooks 5850 mass flow controllers. The main constituents of the outlet gas stream, methane, ethane, ethylene, propylene, butane, butene, benzene, toluene, and xylene were quantified using an Agilent 6890A series gas chromatograph (GC) equipped with a 30 m, 0.53 mm outer diameter J&W Scientific GS-Alumina (115–3532) capillary column connected to a flame ionization detector (FID), which was calibrated with individual product gases.

Propane flow rates were set high enough to avoid the diffusion-controlled regime, and space time was varied by using different catalyst weights. Reactions with the same space time but different combinations of catalyst loadings and reactant flow rates were performed to verify the absence of bulk diffusion. Pore diffusion in ZSM-5 has been reported to take place primarily through the shorter, straight pore perpendicular to the (0 1 0) surface, supporting the use of one-dimensional plate geometry for effectiveness factor calculations [38]

$$\eta = \frac{\tanh\varphi}{\varphi}, \quad \varphi = R\sqrt{k/D} \tag{1}$$

Haag et al. [38] demonstrated that the observed diffusivity of a linear hexene molecule inside the HZSM-5 pore is about 1.5×10^{-3} cm^2/s, which significantly exceeds the Knudsen diffusivity that was estimated to be $\ll 2 \times 10^{-4}$ cm^2/s for hexene. We assumed that this trend would be consistent across the hydrocarbon system of interest and used the typical Knudsen diffusivity value of 10^{-4} cm^2/s, in our calculations to obtain the upper limit of φ. Solving Eq. (1) using the rate constant of alkane carbenium activation as k (Table 4) and a value of 200 nm for the crystallite radius, R, leads to Thiele modulus, $\varphi < 0.01$ confirming the overall kinetic control in the operating range.

Replicate data points were obtained to ensure reproducibility, and the first kinetic measurement was repeated at the end of a series of runs to check for catalyst deactivation. In order to reduce deactivation, the gallium-modified materials were treated with H_2 at 530 °C in between kinetic runs. A dataset with roughly 1450 data points, including variations in temperature, space time, and gallium content, was obtained to study the mechanistic implications of gallium addition. The proton model was fit to a dataset with over 750 data points including temperature and space time variations over HZSM-5.

2.2. Kinetic modeling and parameter estimation

The reaction system was described by an elementary-step-based model that was translated to a set of differential algebraic equations (DAE) via the reaction modeling suite (RMS) [1]. The reactions were parameterized in terms of activation energy and the reference rate constant instead of the pre-exponential factor to avoid correlated parameters. Rate constants were calculated as follows:

$$k_T = k_{ref}\exp\left(-\frac{E_a}{R} * \left(\frac{1}{T} - \frac{1}{T_{ref}}\right)\right) = A\exp\left(-\frac{E_a}{RT}\right) \tag{2}$$

Model fitting and parameter estimation were performed on an in-house package called the reaction modeling suite (RMS) [39,40]. It includes a differential algebraic equation (DAE) generator that writes the equations representing the differential material balances for a given sequence of elementary kinetic steps, a DASSL-based DAE solver, and a parameter estimation package. The parameter estimator used for this work was a hybrid search technique involving a Genetic Algorithm-based search of the full parameter space to identify viable initial guesses, followed by a local optimization in the vicinity of each GA-predicted initial guess. During the fitting process, the reference rate constants (k_{ref}) were constrained within known chemical and physical bounds based on the kinetic theory of gases and thermodynamics.

Statistically meaningful fitting criteria, essential to derive useful information from the data, were included by the replacement of R^2 values by the likelihood criterion as the objective function. This likelihood function represents the probability distribution for the errors in predictions of all the measured product species together as a function of the model parameters. Since using the logarithm of the likelihood function helps reduce the nonlinearity of the optimization routine, the log likelihood function (LLF) was employed as the objective function in the analysis presented here. Error was modeled with a heteroscedasticity parameter that ensured that contributions from experimental error did not obscure the parameter analysis [41]. The statistical error model is described by:

$$\sigma_j^2 = \omega_j^2 \times f_j(X_j)^{\gamma} \tag{3}$$

where σ_j is the standard deviation for the jth measured species and γ, the heteroscedasticity parameter, and ω_j are error model parameters. γ values of 0 and 2 correspond to data with constant error and constant relative error, respectively. Our kinetic data, like most other experimental data, suggest a γ value between 0 and 2. For a maximum value of LLF, we apply $\left(\frac{\partial LLF}{\partial \gamma}\right)_{\omega} = 0$ to obtain

$$\omega_j = \sum_{i=1}^{n} \frac{(y_{ij} - f_j(X_j))^2}{f_j(X_j)^{\gamma}} \tag{4}$$

where j represents the different measured species and n represents the number of data points. The term $f_j(X_j)$ is the model prediction for the jth species at the ith data point and y_{ij} is the measured value for the data point. Eq. (4) has been incorporated in the models to reduce the number of error model parameters.

3. Results and discussion

3.1. Experimental data

As discussed above, gallium-modified materials were reduced in H_2 at 530 °C prior to reaction to allow the large hydrated gallium species to enter into the pores. Ga/HZSM-5 samples with a Ga/Al ratio of 1 were probed using X-ray photoelectron spectroscopy (XPS) and results showed a Ga/Si ratio of 0.13 prior to reduction and that of 0.05 on reduction. Atomic absorption spectroscopy on these materials indicated a bulk Ga/Si ratio of 0.06, therefore, confirming that Ga resides primarily on the external surface of the catalyst prior to reduction and migrates into the pores on reduction.

Kinetic experiments indicated that propane activity, as well as selectivity to aromatics, maximized at a Ga/Al ratio of about 0.5, corresponding to 3.26 wt.% Ga in the zeolite (Fig. 3). The selectivity of any component is defined as the weight percentage of the component in the hydrocarbon product stream. It was observed that the propylene selectivity increased with gallium content while the fuel gas selectivity decreased with increasing gallium content. Similar observations were reported by other researchers such as Rane et al. [49]. The experimental results thus point toward a synergy between proton and gallium sites. Room temperature FT-IR spectra of the reduced Ga/HZSM-5 materials show a decrease in the 3610 cm^{-1} band area with increasing Ga content as shown in Fig. 4. These results suggest an increase in dehydrogenation ability and a decrease in the number of acid sites of the catalyst with increasing gallium content, confirming that Ga promotes dehydrogenation and that it replaces proton sites. The FT-IR spectra also showed the presence of some residual Brønsted acidity even for the over-exchanged Ga/HZSM-5 sample, implying that the nominal 100% exchanged material had only 85% of the gallium in Brønsted

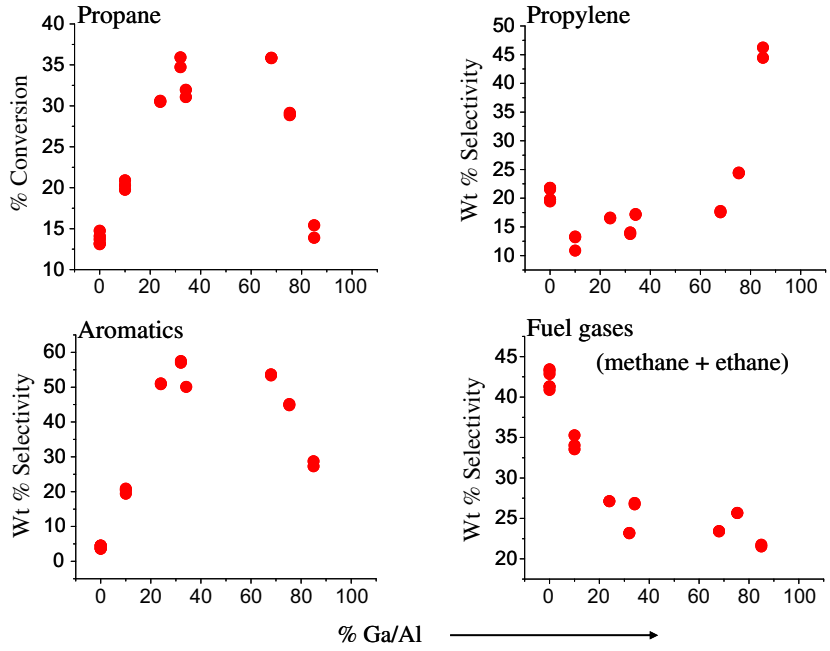

Fig. 3. Experimental observations: Si/Al = 16, T = 530 °C, space time = 1.514 g_{cat} h/mol.

acid positions. We have incorporated this feature in our experimental data by shifting the data points at Ga/Al of 1 to a ratio of 0.85. This disagreement between the elemental analysis and the FT-IR spectra was noticed only for the over-exchanged material. While it is likely that the rest of the gallium may remain in the ZSM-5 pores as entrapped GaO_x species, we have ignored the catalytic activity of such excess gallium species in our kinetic models owing to the low concentrations in which they are present as well as their expected low activity [19,21]. Carbon balances on the gallium-modified materials indicated that 75–95% of the carbon was accounted for. These catalysts were found to be less stable than the parent HZSM-5 and deactivation had to be accounted for in the Ga kinetic models to account for the carbon lost to coke, as will be discussed in the next section.

3.2. Kinetic model development

We have employed microkinetic modeling as a tool to elucidate the chemical nature and role of gallium in Ga/HZSM-5. Two primary functions are present on the gallium-promoted catalyst: a dehydrogenation function associated with gallium and an acid function associated with the Brønsted acid sites not replaced by Ga. A mechanistic description of both functions is included in the kinetic model.

3.2.1. Acid function

Earlier, we developed a reaction mechanism for the aromatization of propane over the fully protonated base catalyst, HZSM-5 [42]. With some minor improvements added since that publication, this model consists of 312 elementary steps including the initial activation of propane via carbonium ion formation and further protolytic dehydrogenation and cracking to form olefins, as proposed by Haag et al. [48]. Further reactions, such as adsorption, desorption, β-scission, oligomerization, hydride transfer, alkyl-

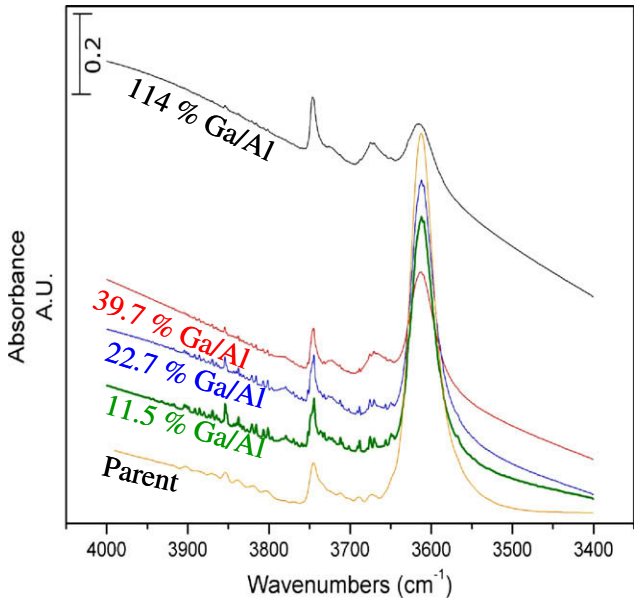

Fig. 4. FT-IR spectra of reduced Ga/HZSM-5 samples at room temperature, Si/Al = 16.

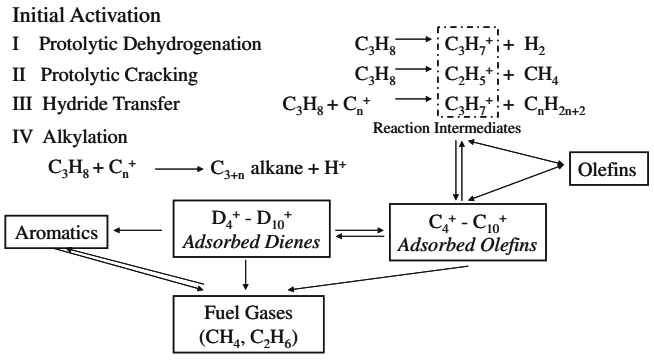

Fig. 5. Details of proton microkinetic model: 312 reaction steps, 38 reaction families, 25 parameters, and 10 rate constants.

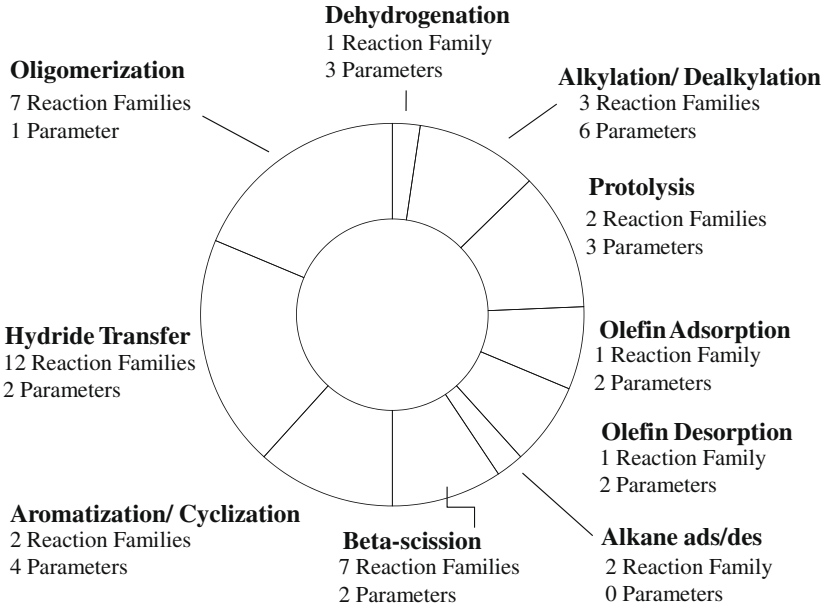

Fig. 6. Summary of proton kinetic model.

ation, dealkylation, and cyclization, take place to make aromatics and hydrogen, as shown in Fig. 5. The reactions were parsed into 38 reaction families involving an equal reactivity assumption based on similarities in reactants, products, and transition states as summarized in Fig. 6 and Table 1b. The system was described with 25 parameters corresponding to 10 rate and equilibrium constants, and the activation energies were found to be in good correspondence with literature predictions, as shown in Table 1a. During the fitting process, pre-exponential factors were constrained within known chemical and physical bounds based on transition state theory and thermodynamics. Fig. 7 shows that good predictions were obtained for measured product concentrations as a function of space time and temperature variations.

Due to the large dimensionality of the overall Ga/HZSM-5 microkinetic model, the parameters describing the proton activity are kept fixed at their optimum values (Table 1a) during the gallium kinetic modeling described later in this paper.

Table 1a
HZSM-5 parameter estimates: 4 of 25 parameters associated with carbon number dependence. Pre-exponential factors in bold represent bimolecular reactions and others represent unimolecular reactions.

Reaction type	$\log_{10}(A)$ (s^{-1} or $(Pa\ s)^{-1}$)	E_{act} (kJ/mol)
Protolytic cracking	10.6	163
Protolytic dehydrogenation	10.0	157
β-Scission (2° → 2°)	12.9	144
Dealkylation	9.6	177
Cyclization	9.6	43.1
Alkene adsorption	**−0.9**	84.2
Hydride transfer (2° → 2°)	**2.2**	98.2
Alkylation	**1.2**	82.8
Aromatization	**3.9**	59.5
	Parameter	Model result
Oligomerization	$\Delta S/R$	15.5
Alkene desorption	ΔH (kJ/mol)	21.2

Table 1b
Parameters associated with proton model rate and equilibrium constants. Equilibrium constants highlighted in bold (k_{ref}: rate constant at T_{ref}, E_{act}: activation energy, ΔE_{act}: carbon number dependence of activation energy).

Reaction type	Parameters
Protolytic cracking	k_{ref}, E_{act}, ΔE_{act}
Protolytic dehydrogenation	k_{ref}, E_{act}, ΔE_{act}
β-Scission	k_{ref}, E_{act}
Dealkylation	k_{ref}, E_{act}, ΔE_{act}
Cyclization	k_{ref}, E_{act}
Alkene adsorption	k_{ref}, E_{act}
Hydride transfer	k_{ref}, E_{act}
Alkylation	k_{ref}, E_{act}, ΔE_{act}
Aromatization	k_{ref}, E_{act}
Oligomerization	$\Delta S/R$
Alkene desorption	k_{ref}, ΔH

3.2.2. Dehydrogenation function

The primary focus of this work is to determine the chemical nature of the gallium active site and the functionality associated with it. While the addition of gallium improves the dehydrogenation capacity of the catalysts, it also reduces the unique deactivation resistance that the parent HZSM-5 possesses. Although we maintain a reducing environment over the catalyst in between kinetic runs, there was some coke formation on these materials. Data suggest that with increasing propane conversion, coke deposition increases linearly. We have developed a simplified coking model that assumes that propane goes to coke, thereby accounting for the carbon lost to coke and closing the carbon material balance. The linear relationship between coke deposition and propane conversion was further used to estimate the rate constant for the coking reaction. For the aromatization reactions, we have proposed two types of active sites – gallium monohydride (GaH^{2+}) and gallium dihydride (GaH_2^+). This section covers microkinetic models based on these two sites. We first consider each site individually and then show that it takes both sites together to fit the experimental data across the full range of Ga loading.

3.2.2.1. Gallium dihydride site (GaH_2^+). The gallium dihydride site (Fig. 8) has often been cited in the literature as the sole active gallium site [19,24,43–45] and involves the replacement of a single proton site by a single gallium atom. During Ga modeling, the activity of each Brønsted acid site not replaced by Ga was described by the 25 parameter proton model with parameters fixed

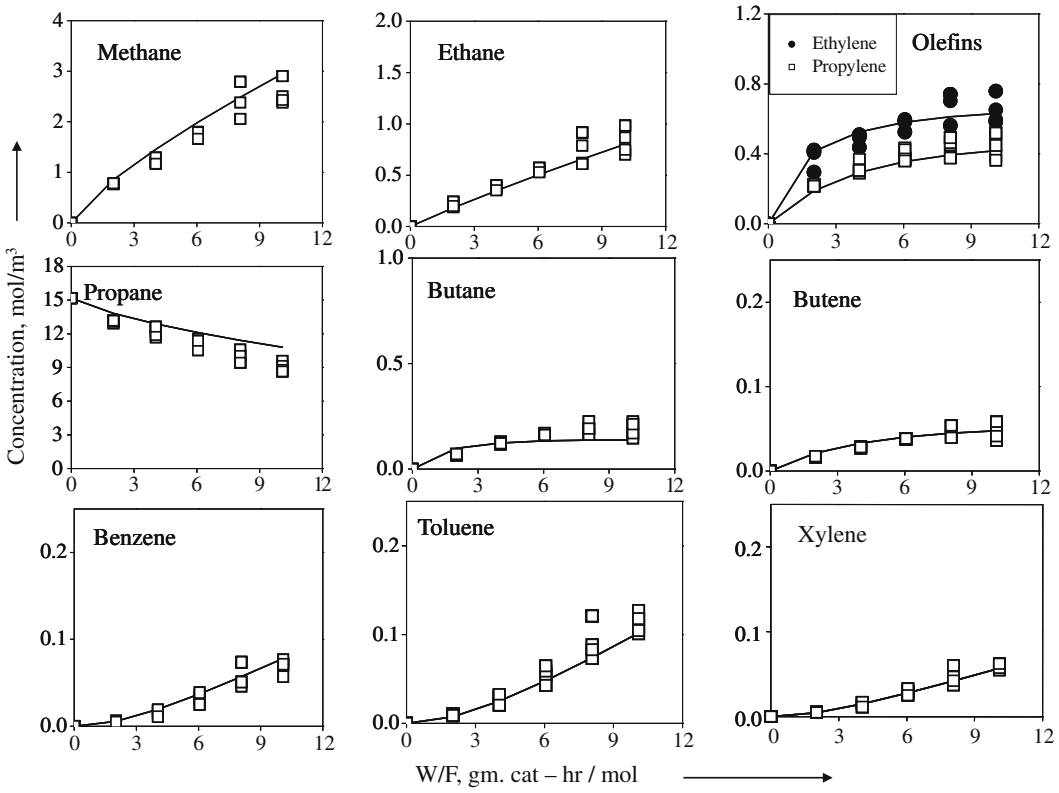

Fig. 7. HZSM-5 model predictions: Si/Al = 16, T = 530 °C.

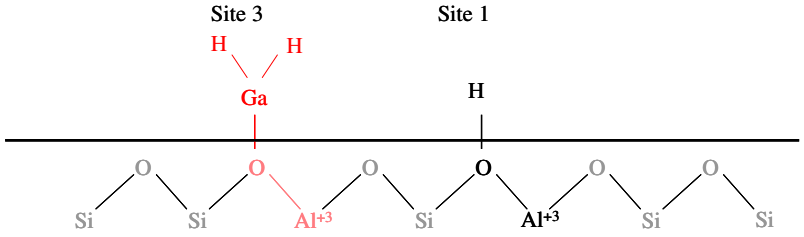

Fig. 8. Gallium dihydride (GaH_2^+) site.

at their optimum values (Table 1a). The number of proton and gallium sites was calculated based on the measured Ga/Al ratio and accounted for in the site balance equations. IR spectra of materials with Ga/Al of 1 suggest 85% exchange (Fig. 4) and therefore for those materials, a Ga/Al ratio of 0.85 was used to calculate the number of proton and gallium sites. The sites were considered independently in the model; however, they influence each other in terms of the concentration of the gas phase species.

A gallium dihydride model consisting of 133 reactions and 18 parameters corresponding to 8 rate constants was developed. The parameters associated with each rate constant are shown in Table 2b. The reactions include alkane adsorption, hydrocarbon activa-

Table 2a
Gallium dihydride model parameters: 2 of 18 parameters associated with carbon number dependence. Pre-exponential factors in bold represent bimolecular reactions and others represent unimolecular reactions.

Reaction type	$\log_{10}(A)$ (s^{-1} or (Pa s)$^{-1}$)	E_a (kJ/mol)
Alkane dehydrogenation	9.48	132
Alkane C–C bond cleavage	8.45	126
Naphthene, olefin dehydrogenation	12.36	146
Olefin adsorption	**0.99**	75.5
Olefin desorption	16.04	79.9
Naphthene, olefin hydrogenation	**1.89**	73.4
Alkane alkylation	**5.29**	107
Aromatic alkylation	**3.94**	42.3

Table 2b
Parameters associated with gallium dihydride model rate constants (k_{ref}: rate constant at T_{ref}, E_{act}: activation energy, ΔE_{act}: carbon number dependence of activation energy).

Reaction type	Parameters
Alkane dehydrogenation	k_{ref}, E_{act}
Alkane C–C bond cleavage	k_{ref}, E_{act}
Naphthene, olefin dehydrogenation	k_{ref}, E_{act}
Olefin adsorption	k_{ref}, E_{act}
Olefin desorption	k_{ref}, E_{act}, ΔE_{act}
Naphthene–olefin hydrogenation	k_{ref}, E_{act}, ΔE_{act}
Alkane alkylation	k_{ref}, E_{act}
Aromatic alkylation	k_{ref}, E_{act}

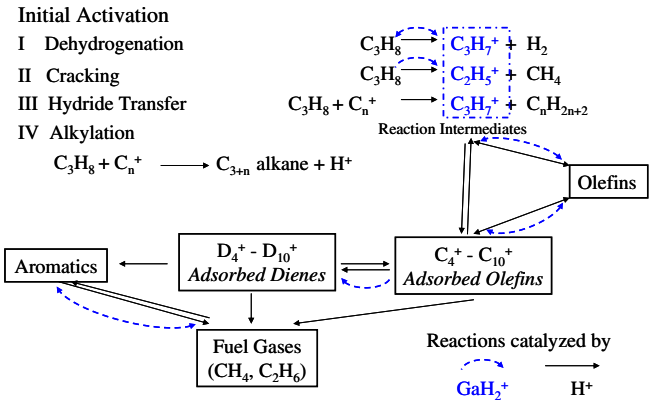

Fig. 9. Gallium dihydride reaction mechanism.

tion, hydrogenation/dehydrogenation, olefin adsorption/desorption, C–C bond cleavage and alkylation/dealkylation as shown in Fig. 9. Several reactions attributed to Ga in the literature have been included in this mechanism. These include DFT studies [44] that proposed that hydrocarbon activation on GaH_2^+ does not take place due to the acidity or basicity of the hydride attached to gallium but that the activity arises due to the C–H and C–C bond polarization in the presence of Ga bonded to the lattice oxygen atoms. C–C cleavage was also assigned to Ga on the basis of ^{13}C MAS NMR experiments by Derouane et al. [46] that attribute fuel gas formation to this reaction. The model incorporating these details was fit to the gallium data, and the activation energies and pre-exponential factors were found to be within the expected ranges (Table 2a).

Model predictions at low and mid-range gallium loadings were found to be in good correspondence with experimental findings as depicted in Fig. 10. However, plots across the full range of gallium contents indicated that this model clearly fails at high gallium loadings, as evident in Fig. 11. This is not surprising since we have assigned all the gallium activity to the gallium dihydride site. As a result, it takes up the high activity at low gallium loadings which perhaps belongs to the gallium monohydride site as described below. In other words, we find that the gallium dihydride site alone cannot describe the activity across the gallium content range.

3.2.2.2. Gallium monohydride (GaH^{2+}) site. The gallium monohydride site (Fig. 12) exists in the vicinity of two near aluminum atoms and requires that one gallium atom annihilates two "nearby" proton sites. The primary motivation for studying this site was recent density functional theory (DFT) findings by Joshi and Thomson [25] that indicated that the dehydrogenation activation energy of 40 kcal/mol associated with this site is more in line with the experimental finding of 39 kcal/mol than the activation energy of 60 kcal/mol associated with the traditional gallium dihydride site (GaH_2^+) [44]. In addition to the gallium monohydride site, we also have Brønsted acid sites with activity per site described by the 25 parameter proton model and parameters fixed to the optimum values obtained as discussed in this paper. "Nearby" aluminum atoms are defined as framework aluminum atoms between 0.4 and 0.6 nm apart [25,29].

The room temperature IR spectra of the reduced Ga/HZSM-5 materials were fit, and the band areas were referenced to the 1880 cm^{-1} band area (–O–Si–O–). The analysis, shown in Fig. 13, indicates that the fall in area is more aligned with the GaH^{2+} site than the GaH_2^+ site at loadings below 50%.

The proton functionality was described by the fixed parameter proton microkinetic model discussed earlier. In this model, all the gallium activity is assigned to the gallium monohydride site, the activity of which is described with a microkinetic model consisting of 52 reaction steps and 16 parameters corresponding to 8 rate constants, as summarized in Fig. 14. The parameters associ-

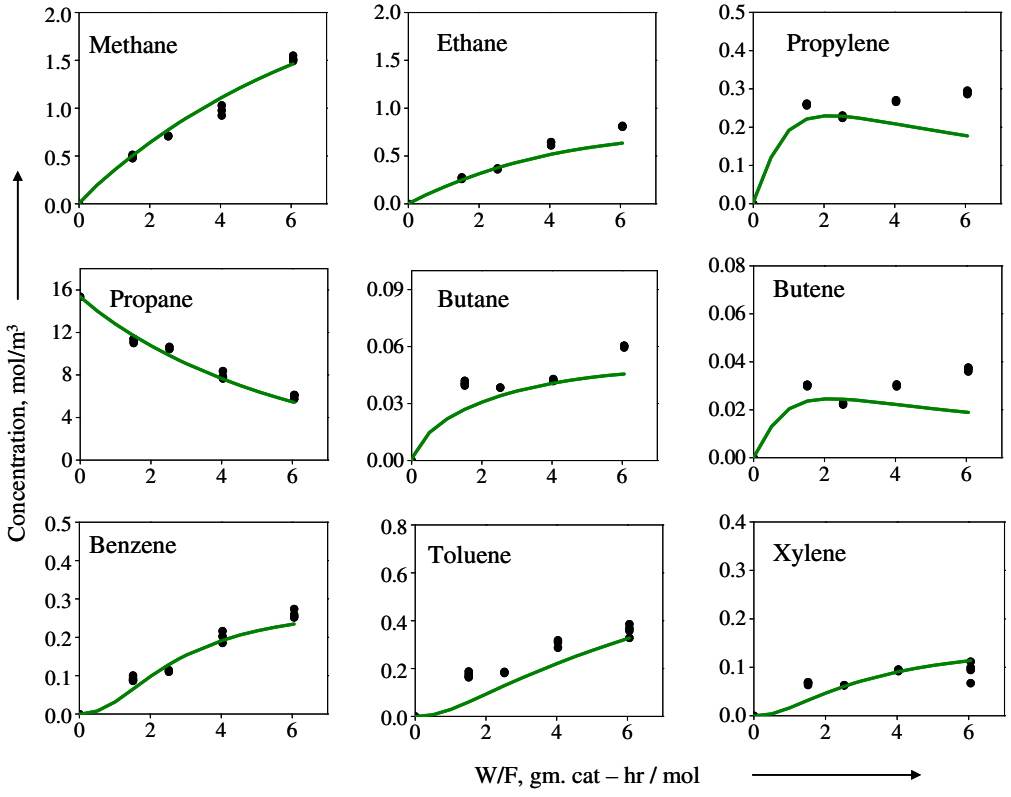

Fig. 10. Gallium dihydride model predictions: Si/Al = 16, Ga/Al = 0.34, T = 520 °C.

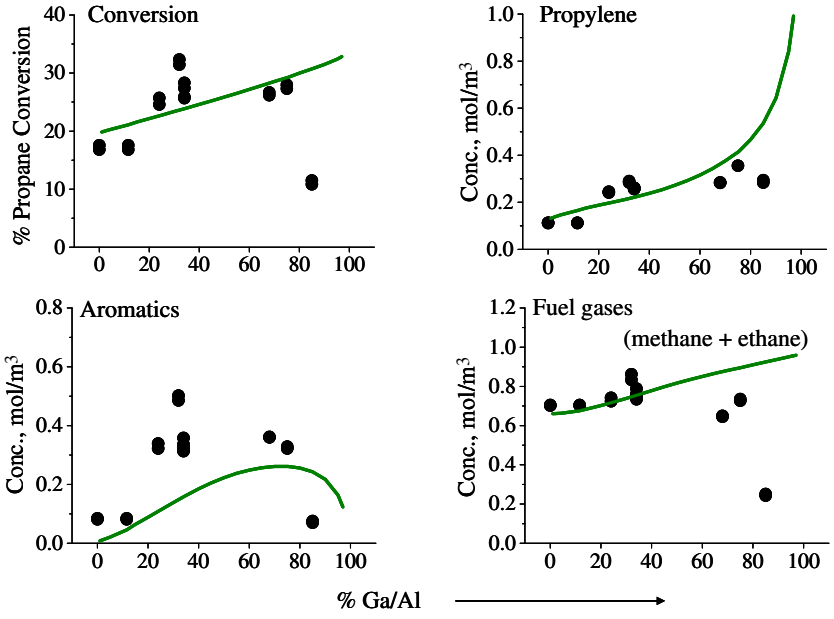

Fig. 11. Gallium dihydride model predictions: Si/Al = 16, space time = 1.514 g_{cat} h/mol, T = 520 °C.

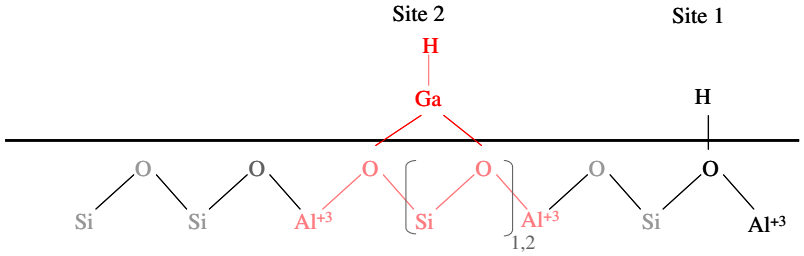

Fig. 12. Gallium monohydride (GaH^{2+}) site.

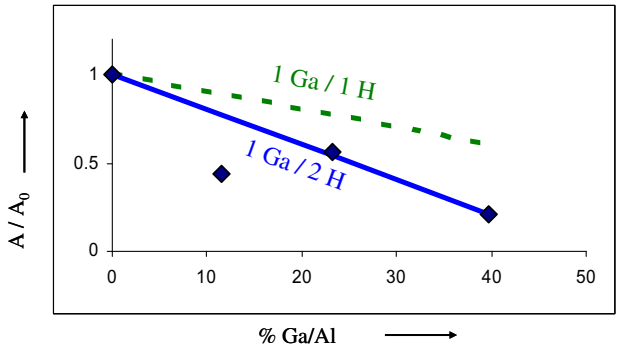

Fig. 13. Room temperature FT-IR spectra of reduced Ga/HZSM-5: A = 3610 cm^{-1} peak area, scaled to the 1880 cm^{-1} framework band.

ated with each rate constant are shown in Table 3b. To begin with, a simplistic assumption that near-Al sites are easily available on the surface of the catalyst was made. This assumption will be relaxed in models described later.

Along the lines of the reaction scheme and terminology proposed by van Santen and coworkers [31], two parallel pathways have been proposed for the activation of hydrocarbons on this site, the first being the "carbenium" activation pathway in which an alkoxide is formed which can then react by carbenium ion chemistry. In this pathway, the hydride from the hydrocarbon adds to the gallium to form a gallium dihydride species (GaH_2^+), which in this mechanism is assigned no intrinsic catalytic activity. The other pathway is the "alkyl" activation pathway in which the alkyl species from the hydrocarbon adds onto the gallium to form H—Ga—$C_3H_7^+$ species. Olefins can desorb from this species to form the gallium dihydride site. In this pathway, the hydride from the hydrocarbon forms the Brønsted acid site that can either react by the carbonium and carbenium ion chemistry or react with a nearby GaH_2^+ site to regenerate the active GaH^{2+} site plus H_2.

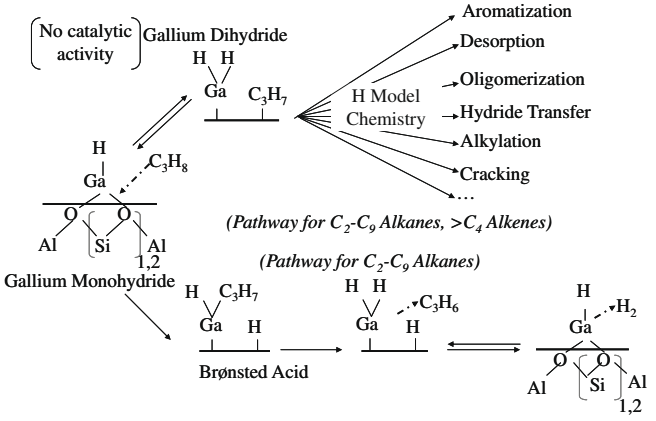

Fig. 14. Reaction mechanism on gallium monohydride (GaH^{2+}) site: 52 reactions, 16 parameters, and 8 rate constants.

Table 3a
Gallium monohydride model (16 parameters) parameter estimates: pre-exponential factors in bold correspond to bimolecular reactions while others correspond to unimolecular reactions.

Reaction type	$\log_{10}(A)$ (s^{-1} or $(Pa\ s)^{-1}$)	E_a (kJ/mol)	E_a (Lit.) [26] (kJ/mol)
Alkane carbenium activation	**5.30**	145	150.6
Regeneration of GaH^{2+} by alkane removal	**5.16**	109	108.8
Regeneration of GaH^{2+} by H_2 removal	**0.01**	42.4	
Formation of GaH_2^+ from GaH^{2+}	**4.71**	93.3	
Alkane alkyl activation	**4.95**	136	136
Olefin desorption from alkyl species	8.24	144	
Alkene carbenium activation	**3.47**	85.1	
Regeneration of GaH^{2+} by alkene removal	**−4.54**	61.4	

Table 3b
Number of parameters associated with gallium monohydride model rate constants (k_{ref}: rate constant at T_{ref}, E_{act}: activation energy).

Reaction type	Parameters
Alkane carbenium activation	k_{ref}, E_{act}
Regeneration of GaH^{2+} by alkane removal	k_{ref}, E_{act}
Regeneration of GaH^{2+} by H_2 removal	k_{ref}, E_{act}
Formation of GaH_2^+ from GaH^{2+}	k_{ref}, E_{act}
Alkane alkyl activation	k_{ref}, E_{act}
Olefin desorption from alkyl species	k_{ref}, E_{act}
Alkene carbenium activation	k_{ref}, E_{act}
Regeneration of GaH^{2+} by alkene removal	k_{ref}, E_{act}

The activation energies obtained by fitting this model to the Ga dataset were in keeping with literature predictions, as shown in Table 3a. However, the pre-exponential factors of reactions such as alkane activation were higher than 10^4 $(Pa\ s)^{-1}$, the upper bound predicted by the kinetic theory of gases [17], suggesting the need for more chemistry in the model. Model predictions were in good agreement with experimental data across both temperature and space time variations, as shown in Fig. 15. Predictions across Ga content (Fig. 16) indicate that the gallium monohydride site chemistry describes the data at most gallium loadings. However, at Ga/Al of 1 when the surface is covered by gallium dihydride sites, the model predicts no propane conversion and therefore no propylene formation. Although we do not have experimental data at 100% proton exchange, other researchers such as Kazansky et al. [27] have shown that there is significant propane conversion to propylene at Ga/Al of 1. In order to capture this feature, some activity needs to be assigned to the gallium dihydride site too.

3.2.2.3. Gallium monohydride–dihydride unified model. So far, we have proposed two types of active sites: gallium dihydride and gallium monohydride and the catalytic functionality associated with each of them. Since no single site was capable of describing all the gallium data, we present here a unified model that brings together the gallium dihydride and monohydride functionalities. Fig. 17 shows a schematic of the surface at different gallium loadings, still assuming that near aluminum pair sites are easily accessible. Initially, the surface is covered by protons. With gallium addition, gallium monohydride sites begin to form until all proton sites have been replaced by gallium. With further gallium addition, each gallium monohydride site splits into two nearby gallium dihydride sites which are assumed not to interact with each other. At a Ga/Al ratio of 1, the surface is covered by gallium dihydride sites. In other words, gallium monohydride sites are formed first but at high loadings, they transform to the gallium dihydride sites.

The reaction mechanism for this unified model is depicted in Fig. 18. The model consists of two pieces; the first is the gallium monohydride functionality which is identical to the one described earlier (Fig. 14) with the "carbenium" and "alkyl" activation pathways. The second piece is the gallium dihydride functionality. In order to reduce the number of parameters in the unified system, we did not incorporate the full gallium dihydride mechanism described in Fig. 9. Instead, we performed a sensitivity analysis on this model by perturbing the model parameters and monitoring the change in the value of the log likelihood function (LLF). The 18 parameter GaH_2 model was fit to the Ga/Al 0.75 dataset where we expect a majority of GaH_2 sites. The changes in individual component LLF, as well as the overall LLF, on perturbing all the parameters together were examined and modeled using JMP 5.0.1. The GaH_2^+ parameters that influence the log likelihood function strongly were deemed significant or well defined by the data when compared to the others and were incorporated in the unified model. The simplified model consists of 10 reaction steps and 6 parameters corresponding to 3 rate constants. In this pathway, the trivalent gallium dihydride site loses hydrogen and forms a univalent gallium (Ga^+) site which can then react with hydrocarbons to lead to the trivalent gallium–alkyl species, H–Ga–$C_2H_5^+$. Olefins can desorb from this species to regenerate the active gallium dihydride site. In this section, we describe the results obtained by fitting this model, assuming that paired aluminum sites are easily available on the surface.

The reaction model consists of 62 reactions and 22 parameters corresponding to 11 rate constants and was fit to the Ga dataset. The model parameters, as reported in Table 4, were found to be in agreement with DFT predictions of Joshi and Thomson [25]. In particular, the "carbenium" activation energy was found to be greater than the "alkyl" activation energy although the difference between them was less than that predicted by Joshi et al. The olefin desorption activation energy from the gallium–alkyl species was found to be 131 kJ/mol, significantly higher than 105 kJ/mol, the activation energy obtained in the 25 parameter proton model for olefin desorption from an alkoxide to regenerate the Brønsted acid site. Our kinetic model parameters are in line with the DFT prediction that the overall "carbenium" pathway is slightly favorable to the overall "alkyl" pathway. The pre-exponential factors of alkane activation reactions on GaH^{2+} were found to be higher than 10^4, the upper bound obtained from calculations based on the kinetic the-

Table 4
Unified model parameter estimates: all Al assumed to be in pairs. Pre-exponential factors in bold correspond to bimolecular reactions while others correspond to unimolecular reactions.

Reaction type	$\log_{10}(A)$ (s^{-1} or $(Pa\ s)^{-1}$)	E_a (kJ/mol)	E_a (Lit.) [25] (kJ/mol)
Alkane carbenium activation on GaH^{2+}	**3.40**	149	150.6
Regeneration of GaH^{2+} by alkane removal	**0.85**	112	108.8
Regeneration of GaH^{2+} by H_2 removal	**5.76**	142	
Formation of GaH_2^+ from GaH^{2+}	**−0.250**	119	
Alkane alkyl activation on GaH^{2+}	**3.19**	142	136
Olefin desorption from alkyl species	7.72	131	
Alkene carbenium activation	**2.79**	108	
Regeneration of GaH^{2+} by alkene removal	**3.17**	177	
Formation of Ga^+ from GaH_2^+	15.8	313	
Regeneration of GaH_2^+ from Ga^+ by H_2 addition	**4.17**	186	
Alkane alkyl activation on Ga^+	**−0.130**	159	

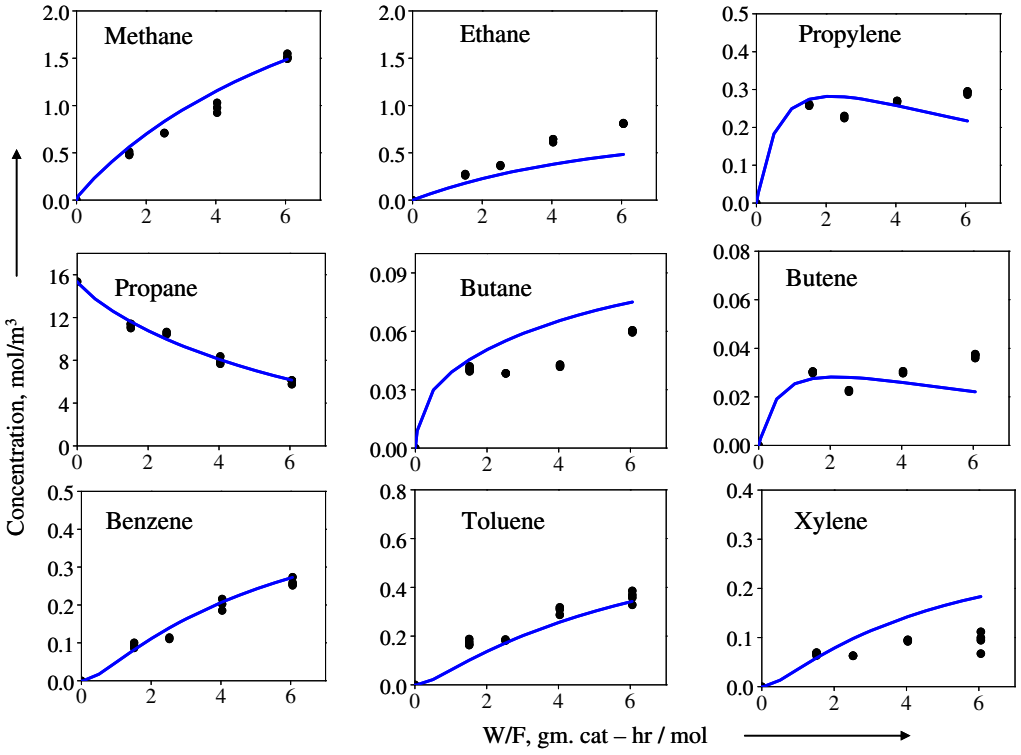

Fig. 15. Gallium monohydride model predictions: Si/Al = 16, Ga/Al = 0.34, T = 520 °C.

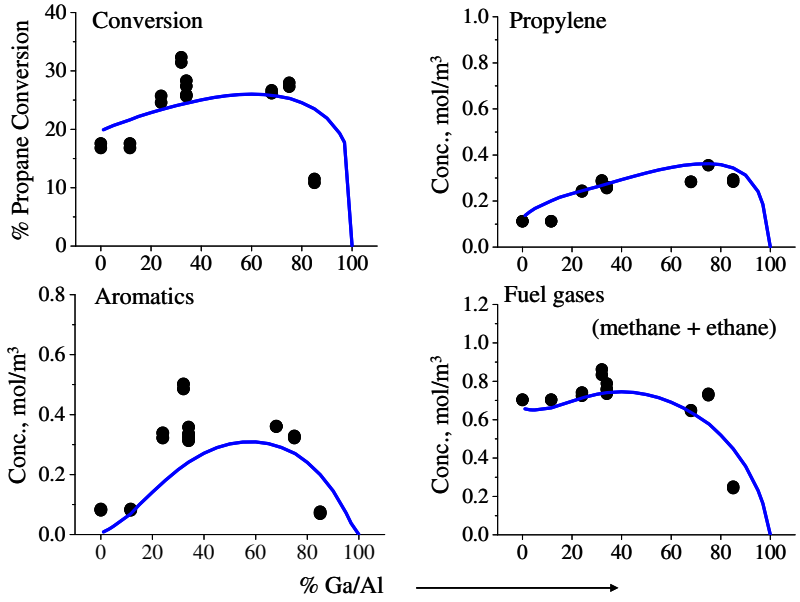

Fig. 16. Gallium monohydride model predictions: Si/Al = 16, space time = 1.514 g_{cat} h/mol, T = 520 °C.

ory of gases, when fit to the GaH^{2+} model alone. The values for these parameters were found to be within bounds in the unified GaH^{2+}–GaH_2^+ model, suggesting that the unified model gives an improved picture of the overall reaction.

The model predictions across temperature, space time, and gallium loading variations are found to be in good agreement with the data. At Ga/Al of 1, the propane conversion is nonzero while propylene selectivity is slightly greater than zero suggesting the low activity of the gallium dihydride site. The formation of aromatics and fuel gases was precluded due to the absence of Brønsted acid sites at Ga/Al of 1. Fig. 19 demonstrates the model performance across Ga/Al ratios and shows that the unified model describes the data at high loadings much better than the models based only on the individual sites. In this unified model, the gallium monohydride (GaH^{2+}) is the predominant active site, while the gallium dihydride (GaH_2^+) takes over at high loadings.

While this model covers all aspects of the data well, it makes the simplistic assumption that near aluminum sites are easily accessible or that all aluminum atoms exist in pairs on the surface of the catalyst. Research has shown that this is not true. Rather

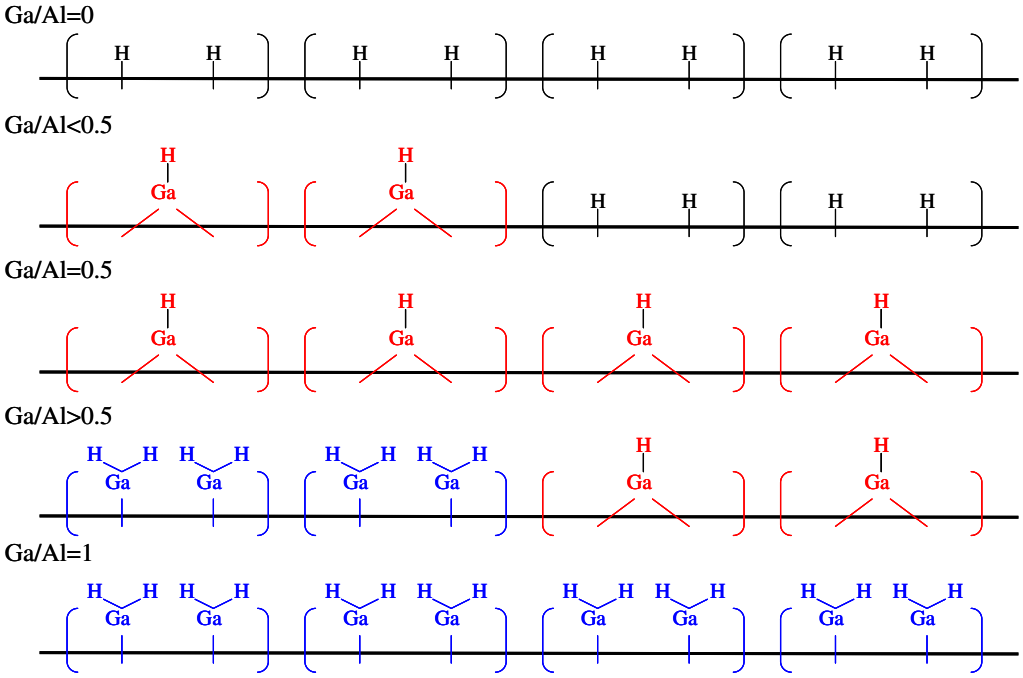

Fig. 17. Schematic of catalyst surface: all aluminums assumed to be in pairs.

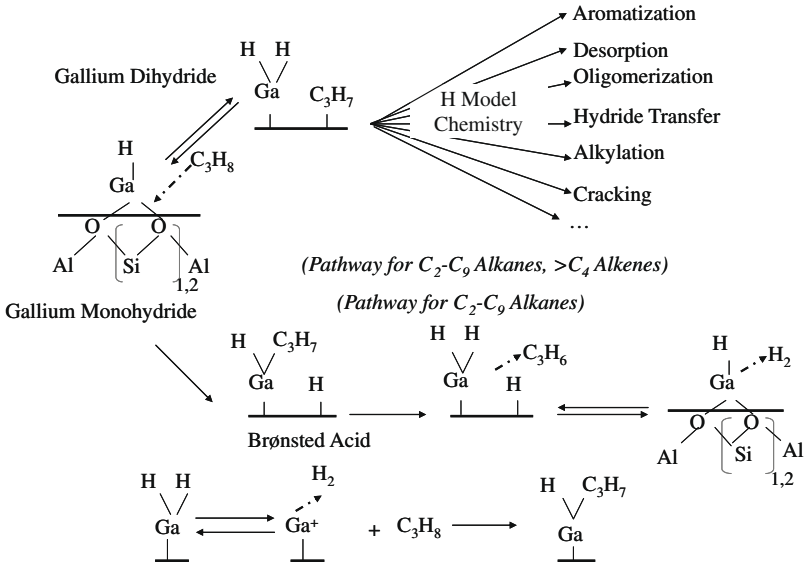

Fig. 18. Unified gallium monohydride–gallium dihydride reaction mechanism: 62 reactions, 22 parameters, 11 rate constants.

there is a distribution of aluminum pair sites on HZSM-5. Notable work includes that of Wichterlova et al. [47], who used Co(II) ions as a probe to indirectly measure the aluminum distribution in HZSM-5. Dehydrated and fully exchanged Co–ZSM-5 materials were studied using UV–vis spectroscopy to monitor the distribution of bare divalent Co(II) ions coordinated exclusively to framework oxygen atoms. They postulate that two nearby AlO_2^- species are needed to balance the positive charge of such cations, thereby relating the number of bare Co(II) species to the number of nearby aluminum atoms on the catalyst. The local coordination of Co(II) at the ion-exchange site was obtained from their d–d transitions in the visible region. Quantitative analysis of the Co(II) spectra yielded three different cationic sites indicative of the bare Co(II) ion, the sum of which provided the number of [Al–O–(Si–O)$_{1,2}$–Al] species. Their results suggest that at a Si/Al ratio of 16, almost 50% of the aluminum atoms in commercial HZSM-5 samples exist in pairs [47].

Another approach to estimate the Al distribution is that of Lercher et al. [51] who characterized Zn-modified Beta zeolites using temperature-programmed desorption (TPD) and IR spectroscopy with pyridine and acetonitrile as probe molecules and reported that Zn^{2+} bridging two nearby Al sites as well as $[Zn–O–Zn]^{2+}$ are likely configurations. An interesting conclusion of this work was the idea that Zn^{2+} or $[Zn(OH)]^+$ cannot be stabilized at isolated Brønsted acid sites and that they migrate into the pore on calcination to regenerate Brønsted acidity.

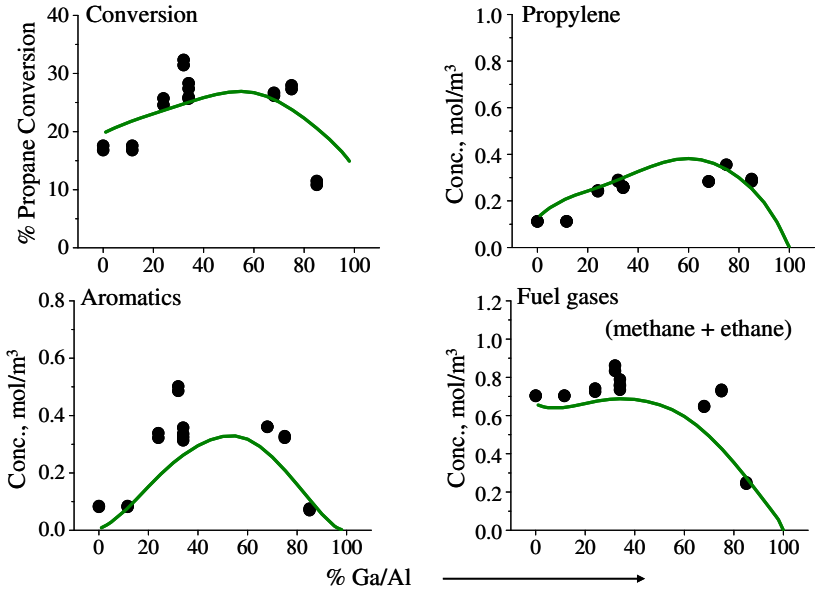

Fig. 19. Unified model predictions: Si/Al = 16: All Al assumed to exist in pairs, Si/Al = 16, T = 520 °C space time = 1.514 g_{cat} h/mol.

If we assume that 50% of aluminum ions in our samples are in pairs, we predict the distribution of GaH_2^+ and GaH^{2+} sites as a function of gallium loading, as shown in Fig. 20. Initially, the surface is covered by Brønsted acid sites. With gallium addition, gallium monohydride sites are formed first until all the dual aluminum protons are replaced by gallium. With further gallium addition, gallium dihydride sites are formed on the isolated aluminum positions, after which the gallium monohydride sites split into two nearby gallium dihydride sites. At a Ga/Al ratio of 1, the surface is covered by gallium dihydride sites (see Fig. 20).

The reaction mechanism described in Fig. 18 was fit to the Ga dataset, and the 50% Al pair model was found to describe the data well, as shown in Fig. 22. The log likelihood function (LLF) of this fit was 1320, lower than the LLF of 1368 obtained by the fit with 100% paired aluminum ions, although in the same range. The 22 parameters obtained for this model (Table 5) show similar activation energies when compared to those from the model which assumed all Al was in pairs (Table 4) as demonstrated in Fig. 21. The pre-exponential factors vary to incorporate changes owing to the new relative numbers of proton, gallium monohydride, and dihydride sites.

We probed the sensitivity of the 22 model parameters by monitoring the change in the objective function (log likelihood function) of individual components as well the overall log likelihood

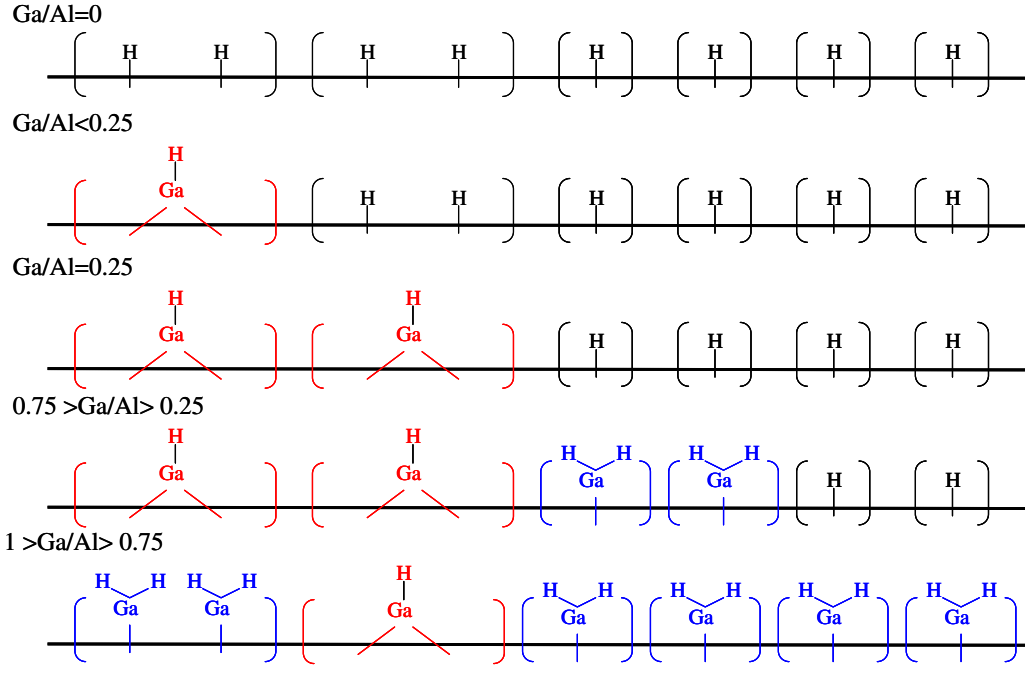

Fig. 20. Schematic of catalyst surface: 50% of aluminums assumed to be in pairs.

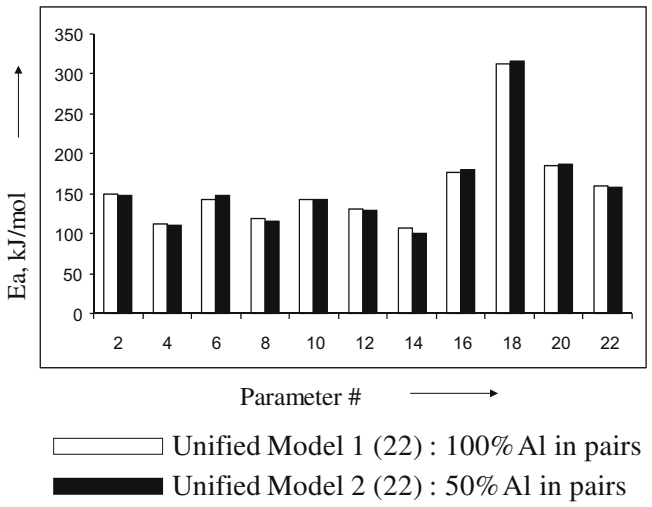

Fig. 21. Effect of percentage paired Al on unified gallium monohydride–gallium dihydride model activation energies.

function with perturbations in parameter values. The parameters that influence the objective function strongly were deemed significant or well defined when compared to the others. It was found that four parameters related to initial alkane activation by the carbenium and alkyl pathways and desorption of olefins from alkyl species like [H–Ga–R] were sensitive suggesting the importance of the initiation steps in the mechanism.

The log likelihood function (LLF) of each of the models described above as fit to the gallium data at a space time of 1.514 g_{cat} h/mol is presented in Table 6. It was found that the GaH_2^+ model has the lowest LLF value and therefore has the poorest fit. The GaH^{2+} model fits the data across Ga content better than the GaH_2^+, while the unified models have the highest LLF values. The unified model assuming that all Al exist in pairs has the highest LLF value and therefore the best fit.

The models were also assessed based on the Akaike information criterion (AIC) [55] and results are shown in Table 6. The AIC is calculated as shown in the following equation:

Table 5
Unified model parameter estimates: 50% of Al assumed to be in pairs. Pre-exponential factors in bold correspond to bimolecular reactions while others correspond to unimolecular reactions.

Reaction type	$\log_{10}(A)$ (s^{-1} or (Pa s)$^{-1}$)	E_a (U/mol)	E_a (Lit.) [26] (kJ/mol)
Alkane carbenium activation on GaH^{2+}	**4.43**	147.28	150.6
Regeneration of GaH^{2+} by alkane removal	**2.21**	109.70	108.8
Regeneration of GaH^{2+} by H_2 removal	**2.43**	147.05	
Formation of GaH_2^+ from GaH^{2+}	**2.73**	116.16	
Alkane alkyl activation on GaH^{2+}	**4.49**	143.25	136
Olefin desorption from alkyl species	7.25	129.19	
Alkene carbenium activation	**3.54**	100.70	
Regeneration of GaH^{2+} by alkene removal	**4.81**	179.29	
Formation of Ga^+ from GaH_2^+	15.50	316.44	
Regeneration of GaH_2^+ from Ga^+ by H_2 addition	**3.08**	186.33	
Alkane alkyl activation on Ga^+	**3.02**	158.34	

Table 6
Log likelihood function (LLF) and Akaike information criterion (AIC) associated with gallium models: space time = 1.514 g_{cat} h/mol.

Model	Parameters	LLF	AIC
GaH_2^+ model (133 reactions)	18	1197	−2358
GaH^{2+} model (52 reactions)	16	1271	−2510
GaH^{2+}–GaH_2^+ unified model (62 reactions) (all Al assumed to be in pairs)	22	1331	−2618
GaH^{2+}–GaH_2^+ unified model (62 reactions) (50% Al assumed to be in pairs)	22	1283	−2522

$$AIC = 2N - 2LLF \quad (5)$$

The difference between the AIC values (ΔAIC) is used to assess the goodness of the models, where the model with the lowest AIC value is the best model. As shown in Table 6, the GaH^{2+}–GaH_2^+ unified model has a lower AIC than the GaH^{2+} and the GaH_2^+ models, confirming the need for the both steps to describe the data. The

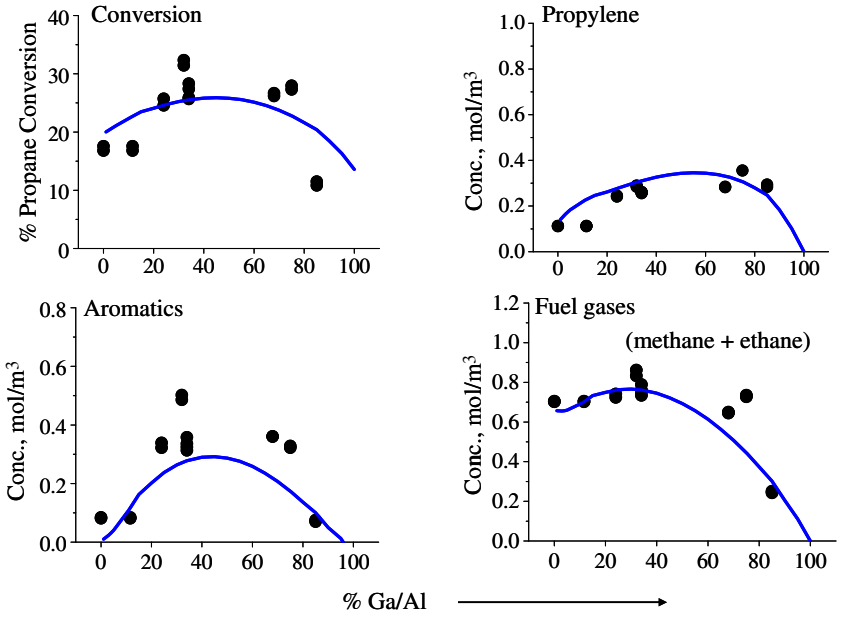

Fig. 22. Unified gallium monohydride–gallium dihydride model predictions: 50% of aluminums assumed to be in pairs, Si/Al = 16, T = 520 °C, space time = 1.514 g_{cat} h/mol.

AIC values of the unified model evaluated at the two bookend scenarios of 100% Al in pairs and 50% Al in pairs are compared to indicate the effect of paired Al sites. It is seen that the model that assumes 100% Al in pairs has a lower AIC and therefore is the best model.

4. Conclusions

Ga/HZSM-5 catalysts were prepared by the incipient wetness impregnation technique with gallium nitrate and pretreated in hydrogen at 530 °C prior to reaction to aid the migration of gallium into the pores. XPS results confirmed that reduction was necessary for this process. Kinetic experiments indicate a peak in propane conversion and aromatics selectivity at Ga/Al of 0.5. Propylene selectivity increases with Ga/Al, confirming a boost in the dehydrogenation function on Ga addition while fuel gas selectivity decreases with increasing Ga/Al suggesting a decrease in the number of acid sites. The fall in number of acid sites was further verified by the reduction in the 3610 cm^{-1} band area with increasing Ga content, in room temperature FT-IR spectra. The experimental data therefore point toward interplay between proton and gallium sites.

An elementary-step-based microkinetic model has been postulated to describe propane aromatization over bifunctional gallium-modified HZSM-5 catalysts. The proton activity per Brønsted acid site was described using 312 elementary steps and 25 rate and equilibrium parameters corresponding to 10 rate constants and was kept fixed during gallium modeling. Kinetic models based on two different Ga active sites, GaH^{2+} and GaH_2^+, were first used individually to describe the diverse dataset of 1450 data points that includes conversion to 10 different products as a function of temperature, space time, and Ga/Al variation. Two parallel pathways, "carbenium" and "alkyl", were proposed for hydrocarbon activation over the gallium monohydride site (GaH^{2+}). The "carbenium" pathway proceeds via the formation of an alkoxide anchored to the zeolite and a gallium dihydride species. The "alkyl" pathway involves the formation of a Brønsted acid site and the gallium–alkyl species. The activation energies obtained are in accordance with findings of Joshi and Thomson [25] While this site was found to describe the dataset at most gallium loadings, it predicts no activity at a Ga/Al ratio of 1 since gallium dihydride sites were assigned no catalytic activity in this model.

A unified GaH_2^+–GaH^{2+} model consisting of 62 reactions and 22 parameters corresponding to 11 rate constants was developed with catalytic functionality assigned to both these sites, and model predictions were found to be in good accord with experimental data. The gallium dihydride activity involves the reduction of the trivalent gallium dihydride species to the univalent Ga^+ that then activates hydrocarbons. We demonstrate this model assuming that (i) near aluminum sites are easily accessible on HZSM-5 with Si/Al ratio of 16 and also that (ii) 50% of the aluminum atoms exist in nearby positions, based on findings of Wichterlova et al. [47]. In these models, no cyclization steps have been assigned to the gallium active sites. The aromatization functionality on the proton sites is found capable of describing the data across Ga variations, supporting the notion that this reaction takes place solely on Brønsted acid sites. The complexity and high dimensionality of the reaction mechanism have precluded the use of Bayesian and other nonlinear approaches to obtain nonlinear confidence intervals on parameter estimates [41]. Although a comparative study of the model parameters requires some knowledge of the nonlinear confidence intervals, we make some general comments on the activation energies obtained. The activation energy for alkane "carbenium" activation was obtained to be 148 kJ/mol, higher than the alkane "alkyl" activation energy of 142 kJ/mol. The olefin desorption activation energy was found to be around 131 kJ/mol from the gallium–alkyl species as opposed to the corresponding value of 105 kJ/mol by the carbenium ion chemistry on the Brønsted acid site. In other words, our model parameters support the DFT finding that the "carbenium" pathway is energetically more favorable than the "alkyl" pathway. Sensitivity analysis of the 22 parameter model indicates the significance of four parameters related to the initial activation of alkanes and conversion to alkenes. We also find that the commonly reported gallium dihydride site (GaH_2^+) alone cannot describe the optimum with Ga/Al, which led to the conclusion that the gallium monohydride site (GaH^{2+}) is also needed.

We propose that the active site for propane aromatization on Ga/HZSM-5 varies with gallium loading and Si/Al ratio. In HZSM-5 materials with low Si/Al ratio, such as ours, the likelihood that aluminums exist in nearby positions (Al–Al distance = 0.4–0.6 nm) is higher. When gallium is added to these materials, we propose that gallium monohydride sites are formed first after which gallium dihydride sites are formed at the isolated aluminum sites. At high Ga/Al ratios, the gallium monohydride site transforms into two gallium dihydride sites to accommodate the additional gallium species. We postulate that the gallium monohydride site (GaH^{2+}) is the predominant active site and the gallium dihydride site (GaH_2^+), with lower activity, takes up the activity at high gallium loadings where gallium monohydride sites are absent. The relative number of GaH^{2+} and GaH_2^+ species is a strong function of the percent paired aluminum atoms in HZSM-5, which will vary with Si/Al ratios and nature of synthesis of the parent HZSM-5. This number is not fit by the data but is provided to the model by the user. On reducing the number of paired Al from 100% to 50%, the model was still found to describe the data well. The activation energies were found to be similar in both cases while pre-exponential factors were found to adjust to incorporate variations in relative number of sites. This is not surprising because the same functionality is now concentrated on fewer sites. Table 6 shows the log likelihood functions (LLF) for both cases and suggests that the unified model which assumes that all the Al is present in near-Al positions has a higher LLF value. In other words, this case describes the data better. Table 6 lists the AIC values associated with the models and also indicates that the all near-Al unified models the best. However, the authors observe that these results cannot be used to determine the relative number of Ga-sites on the surface of the catalyst. We believe that the kinetic model alone is not sufficient to describe the number of paired sites on the catalyst and that it needs to be supplemented with surface characterization data to fully describe the reaction chemistry.

At high Si/Al ratios, we would expect to find fewer aluminum sites within 0.4–0.6 nm from each other and hence the number of gallium monohydride sites would be lower. The gallium dihydride site would be the active site in this case, leading to a lower catalytic activity. Joshi and Thomson [25] propose from DFT findings that at low Si/Al ratios, steric factors reduce the activity of the gallium monohydride sites and, therefore, suggest the presence of an optimum Si/Al ratio in Ga/HZSM-5. A study of gallium-modified HZSM-5 with varying Si/Al ratios would help verify this proposition.

An important feature of this work is the use of microkinetic modeling as a tool to differentiate between possible active sites. Since FT-IR evidence strongly suggests that gallium annihilates proton sites, we have not described here a model that we built assuming the contrary. That model was unable to describe the fuel gas concentrations and the optimum with gallium content. We also note that Ga^+ and GaH_2^+ sites can be considered to have similar microkinetic models in this approach since they replace the proton sites in a similar fashion and are known to catalyze hydrocarbon activation and dehydrogenation by similar pathways. The GaO^+ site suggested by van Santen et al. [24] was also tested to describe the

experimental data at high gallium content. It was found that with suitable functionality, these sites can describe the data at Ga/Al of 1. The $[(H)Ga(OH)_2Ga(H)]^{2+}$ site proposed by van Santen et al. [32] in the presence of steam was not tested against our kinetic data, measured in the absence of steam. Our proposed GaH^{2+}–GaH_2^+ model describes the data at high Ga/Al ratios with Ga^+ and GaH_2^+ sites and is in agreement with spectroscopic evidence for these materials obtained by Subbotina and Kazansky [54]. It was found that any combination of Ga^+, GaH_2^+ and GaO^+ could be used to describe the data at high gallium loadings but none could describe the optimum with gallium content. A site with a structure that involves the annihilation of two proton sites at low Ga/Al and single proton sites at high Ga/Al are needed to describe Ga dependence of our kinetic data. The gallium monohydride site is one site with such a function and is therefore proposed as the predominant active site. The presence of other gallium species with such a function is possible. While the gallium function at high Ga/Al ratios could be described by any of the gallium sites replacing single proton sites, we propose the gallium dihydride site as the predominant site at high Ga loadings based on spectroscopic [23,24] and quantum chemical [25] evidence presented in literature.

Acknowledgments

The authors would like to thank Dr. Yogesh Joshi and Prof. Kendall Thomson for valuable discussions on the density functional theory calculations on these materials. Dr. Shuo-Huan Hsu is acknowledged for advancing the reaction modeling suite (RMS) used in this work. The authors are also grateful to Prof. Gary Blau for providing statistical insights on the models and Steve Stamatis for advice on the AIC calculations. This work was supported by the Department of Energy, Office of the Basic Energy Sciences, through the Catalysis Science Grant No. DE-FG02-03ER15466. We are grateful to ExxonMobil for supplying the HZSM-5 sample used in this study and Dr. James Rekoske from UOP for valuable discussions.

References

[1] J.M. Caruthers, J.A. Lauterbach, K.T. Thomson, V. Venkatasubramanian, C.M. Snively, A. Bhan, S. Katare, G. Oskarsdottir, Journal of Catalysis 216 (2003) 98.
[2] N.Y. Chen, T.Y. Yan, I&EC Process Design and Development 25 (1986) 151.
[3] J.A. Johnson et al., in: NPRA Annual Meeting, Paper AM-84-85, 1984.
[4] M. Guisnet, N.S. Gnep, Applied Catalysis A: General 146 (1996) 33.
[5] W.O. Haag, R.M. Lago, P.B. Weisz, Nature 309 (1984) 589.
[6] M.S. Scurrel, Applied Catalysis 41 (1988) 89.
[7] B.S. Kwak, W.M.H. Sachtler, W.O. Haag, Journal of Catalysis 149 (1994) 465.
[8] D. Barthomeuf, Materials Chemistry and Physics 17 (1987) 49–71.
[9] L. Zhao, J. Zhu, H.Y. Wang, M. Wei, J. Ma, Y.Z. Bai, Petroleum Science and Technology 25 (5–6) (2007) 577.
[10] P. Meriaudeau, C. Naccache, Journal of Catalysis 157 (1995) 283.
[11] G.L. Price, V. Kanazirev, Journal of Catalysis 126 (1990) 267.
[12] P. Chu, US Patent 4,120,910, 1978.
[13] P. Meriaudeau, S.B. Abdul Hamid, C. Naccache, Journal of Catalysis 139 (1993) 683.
[14] B.S. Kwak, W.M.H. Sachtler, Journal of Catalysis 145 (1994) 456.
[15] V.R. Choudhary, K. Mantri, C. Sivadinarayana, Microporous and Mesoporous Materials 37 (2000) 1.
[16] V. Kanazirev, G.L. Price, K.M. Dooley, Journal of the Chemical Society, Chemical Communications 712–713 (1990).
[17] J.A. Dumesic, D.F. Rudd, L.M. Aparicio, J.E. Rekoske, A.A. Trevino, The Microkinetics of Heterogeneous Catalysis, American Chemical Society, Washington, DC, 1993.
[18] H. Kitagawa, Y. Sendoda, Y. Ono, Journal of Catalysis 101 (1986) 12.
[19] K.M. Dooley, G.L. Price, V.I. Kanazirev, V.I. Hart, Catalysis Today 31 (1996) 305.
[20] V.R. Choudhary, P. Devadas, S. Banerjee, A. Kinage, Microporous and Mesoporous Materials 47 (2001) 253.
[21] G.J. Buckles, G.J. Hutchings, Catalysis Today 31 (1996) 233.
[22] J.A. Biscardi, E. Iglesia, Journal of Catalysis 182 (1999) 117.
[23] G.D. Meitzner, E. Iglesia, J.E. Baumgartner, E.S. Huang, Journal of Catalysis 140 (1993) 209.
[24] N. Rane, A.R. Overweg, V.B. Kazansky, R.A. van Santen, E.J.M. Hensen, Journal of Catalysis 239 (2) (2006) 478.
[25] Y.V. Joshi, K.T. Thomson, Journal of Catalysis 246 (2007) 249.
[26] V.B. Kazansky, I.R. Subbotina, R.A. van Santen, E.J.M. Hensen, Journal of Catalysis 227 (2) (2004) 263.
[27] V.B. Kazansky, I.R. Subbotina, R.A. van Santen, E.J.M. Hensen, Journal of Catalysis 233 (2) (2005) 351.
[28] E.J.M. Hensen, M. Garcia-Sanchez, N. Rane, et al., Catalysis Letters 101 (1–2) (2005) 79.
[29] E.A. Pidko, V.B. Kazansky, E.J.M. Hensen, R.A. van Santen, Journal of Catalysis 240 (2006) 73.
[30] I.V. Kuzmin, G.M. Khidomirov, E.J.M. Hensen, Catalysis Letters 108 (3–4) (2006) 187.
[31] E.A. Pidko, E.J.M. Hensen, R.A. van Santen, Journal of Physical Chemistry C 111 (35) (2007) 13068.
[32] E.J.M. Hensen, E.A. Pidko, N. Rane, R.A. van Santen, Angewandte Chemie – International Edition 46 (38) (2007) 7273.
[33] J.A. Biscardi, E. Iglesia, Catalysis Today 31 (1996) 207.
[34] Meriaudeau, C. Naccache, Catalysis Letters 32 (1995) 235.
[35] M. Garcia-Sanchez, P.C.M.M. Magusin, E.J.M. Hensen, P.C. Thune, R.A. van Santen, Journal of Catalysis 219 (2003) 352.
[36] K.M. Dooley, C. Chang, G.L. Price, Applied Catalysis A: General 84 (1992) 17.
[37] D.B. Lukyanov, T. Vazhnova, Journal of Physical Chemistry B 110 (2006) 18473.
[38] W.O. Haag, R.M. Lago, P.B. Weisz, Faraday Discussions of the Chemical Society 72 (1981) 317.
[39] S. Katare, J.M. Caruthers, W.N. Delgass, V. Venkatasubramanian, Industrial & Engineering Chemistry Research 43 (14) (2004) 3484.
[40] S. Katare, A. Bhan, J.M. Caruthers, W.N. Delgass, V. Venkatasubramanian, Computers & Chemical Engineering 28 (12) (2004) 2569.
[41] G.E. Blau, M. Lasinski, S. Orcun, S.-H. Hsu, J.M. Caruthers, W.N. Delgass, V. Venkatasubramanian, Computers & Chemical Engineering 32 (4–5) (2008) 971.
[42] A. Bhan, S.-H. Hsu, G.E. Blau, J.M. Caruthers, V. Venkatasubramanian, W.N. Delgass, Journal of Catalysis 235 (1) (2005) 35.
[43] D.B. Lukyanov, T. Vazhanova, Applied Catalysis A: General 316 (1) (2007) 61.
[44] M.V. Frash, R.A. van Santen, Journal of Physical Chemistry A 104 (2000) 2468.
[45] I.V. Kuzmin, G.M. Zhidomirov, V.N. Solkan, International Journal of Quantum Chemistry 107 (13) (2007) 2434.
[46] I. Ivanova, N. Blom, E.G. Derouane, Journal of Molecular Catalysis A: Chemical 109 (1996) 157.
[47] J. Dedecek, D. Kaucky, B. Wichterlova, Chemical Communications 970 (2001).
[48] W.O. Haag, Studies in Surface Science and Catalysis 84 (1994) 1375.
[49] N. Rane, M. Kersbulck, R.A. van Santen, E.J.M. Hensen, Microporous and Mesoporous Materials 110 (2008) 279.
[50] J. Bandiera, Y.B. Taarit, Applied Catalysis A 152 (1997) 43.
[51] J. Penzien, A. Abraham, J.A. van Bokhoven, A. Jentys, T.E. Muller, C. Sievers, J.A. Lercher, Journal of Physical Chemistry B 108 (2004) 4116.
[52] I.V. Kuzmin, G.M. Zhidomirov, V.N. Solkan, V.B. Kazansky, Kinetics and Catalysis 50 (5) (2009) 752.
[53] E.A. Pidko, R.A. van Santen, E.J.M. Hensen, Physical Chemistry Chemical Physics 11 (16) (2009) 2893.
[54] I.R. Subbotina, V.B. Kazansky, Petroleum Chemistry 49 (1) (2009) 11.
[55] H. Akaike, IEEE Transactions on Automatic Control 19 (6) (1974) 716.